NANO LETTERS

Letter

pubs.acs.org/NanoLett

Low-Temperature Processed Electron Collection Layers of Graphene/TiO_2 Nanocomposites in Thin Film Perovskite Solar Cells

Jacob Tse-Wei Wang,[†] James M. Ball,[†] Eva M. Barea,[‡] Antonio Abate,[†] Jack A. Alexander-Webber,[†] Jian Huang,[†] Michael Saliba,[†] Iván Mora-Sero,[‡] Juan Bisquert,[‡] Henry J. Snaith,*[,†] and Robin J. Nicholas*[,†]

[†]Department of Physics, Clarendon Laboratory, University of Oxford, Parks Road, Oxford OX1 3PU, United Kingdom

[‡]Photovoltaic and Optoelectronic Devices Group, Department de Física, Universitat Jaume I, 12071 Castelló, Spain

Supporting Information

ABSTRACT: The highest efficiencies in solution-processable perovskite-based solar cells have been achieved using an electron collection layer that requires sintering at 500 °C. This is unfavorable for low-cost production, applications on plastic substrates, and multijunction device architectures. Here we report a low-cost, solution-based deposition procedure utilizing nanocomposites of graphene and TiO_2 nanoparticles as the electron collection layers in meso-superstructured perovskite solar cells. The graphene nanoflakes provide superior charge-collection in the nanocomposites, enabling the entire device to be fabricated at temperatures no higher than 150 °C. These solar cells show remarkable photovoltaic performance with a power conversion efficiency up to 15.6%. This work demonstrates that graphene/metal oxide nanocomposites have the potential to contribute significantly toward the development of low-cost solar cells.

KEYWORDS: *Graphene, TiO_2, perovskite, hybrid photovoltaics, nanocomposites*

Thin-film photovoltaics aim to reduce the cost per unit energy of electricity generated from sunlight compared to conventional silicon solar cells. Several approaches have been developed for solar cells such as amorphous and nanocrystalline Si,[1] inorganic compound semiconductors,[2,3] quantum dot solar cells (QDSCs),[4] dye-sensitized solar cells (DSSCs),[5] organic solar cells (OSCs),[6] and now perovskite-based meso-superstructured solar cells (MSSCs).[7] In particular, solid-state perovskite-based solar cells have risen to the forefront of emerging PV research.[7−12] Evolving from DSSCs, MSSCs have demonstrated remarkably high power conversion efficiency of over 12%, broad light absorption, and open-circuit voltages (V_{oc}) of over 1.1 V, by employing an organometal halide perovskite, $CH_3NH_3PbI_{3-x}Cl_x$, as the absorber, coated upon the surface of a mesoporous alumina scaffold. Perovskite absorbers are also desirable by virtue of being easy to solution-process at low temperature using low-cost materials and do not rely on the use of elements in limited supply, unstable solvents such as hydrazine, and high-temperature annealing. In the most efficient thin-film solar cells, electron-collection layers also play a vital role by facilitating selective charge collection. For most commercial thin film solar cells, CdS is used for this purpose, however it significantly contributes to parasitic absorption in the solar cell and additionally contains nondesirable Cd.[13] Metal oxide materials such as TiO_2 and ZnO are widely used in most studies on emerging technologies because they can prevent shunting and leakage currents under reverse bias.[14] But such materials still require high-temperature processing to increase their crystallinity and achieve suitably high charge carrier mobility.[15] Similarly, this still remains a challenge for MSSCs, as high-temperature sintering of the n-type TiO_2 electron-selective contact is still important for high performance. High-temperature sintering has several drawbacks because it results in higher cost and slower production, and it limits the applications to solid, temperature-resilient substrates, preventing its use with plastic and malleable metal foils and multijunction device architectures.[16] Replacing the sintered TiO_2 compact layers should make the perovskite solar technology as versatile in its deployment as organic photovoltaics. Several approaches have been reported in order to achieve comparable electronic properties for the n-type collection layers in other solar technologies, such as atomic layer deposition (ALD), high-pressure pressing, chemical sintering, sol−gel, and electrodeposition.[17−21] Up to now, these alternative methods have not yet achieved an equivalent performance to the conventional high-temperature process, due to crack formation in the film, poor adhesion to the substrate,

Received: October 25, 2013
Revised: November 27, 2013

dx.doi.org/10.1021/nl403997a | *Nano Lett.* XXXX, XXX, XXX−XXX

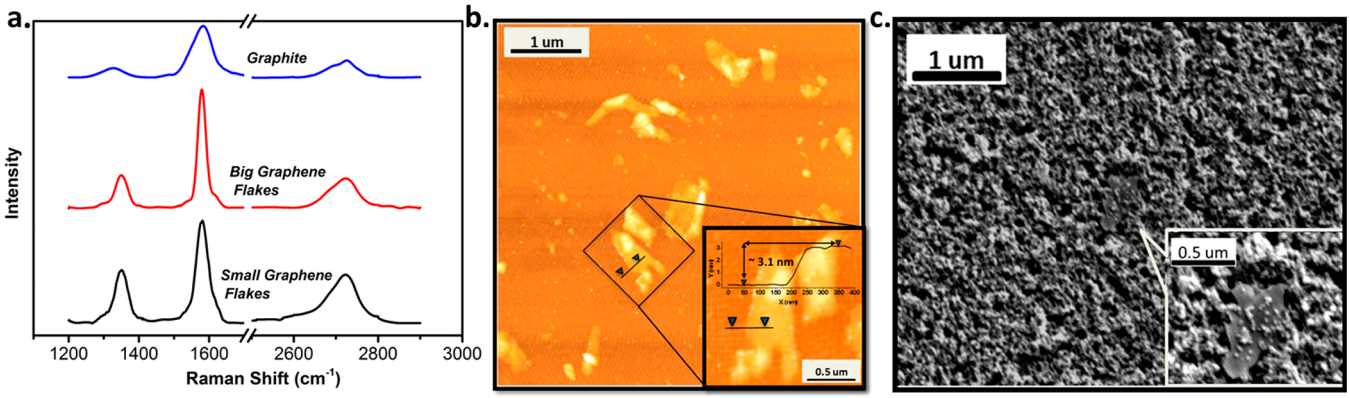

Figure 1. (a) Raman spectra of starting graphite flakes and its exfoliated graphene deposited on the SiO_2 substrate with increasing sonication time. (b) AFM image of exfoliated graphene scanned with 5 μm × 5 μm size and enlargement of the graphene flakes and its height profile of the lines shown in the inset figure. (c) SEM images of graphene-TiO_2 nanocomposites with enlargement micrographs in the inset.

unfavorable crystallinity of TiO_2, and a lack of good connectivity between particles.[22,23]

Meanwhile, advances in graphene research have led to numerous fundamental breakthroughs. In this atom-thick two-dimensional (2D) material, charge-carriers mimic relativistic particles with zero mass,[24] which endow it with remarkably high charge mobility and electronic conductivity.[25−27] It has not only been identified as one of the strongest materials,[28] but is also equipped with unique properties ranging from superior thermal conductivity, and high optical transmittance.[29−31] Therefore, it has aroused interest in applications for graphene-based nanocomposites including photovoltaics, photocatalysis, nanoelectronics, sensors, and so forth.[32−36] In particular, in graphene-TiO_2 nanocomposites, exploiting the benefits of high conductivity and better electrical contacts of graphene and graphene-like materials to electron transport has been proposed.[37−40] To date, only reduced graphene oxide (RGO) has been used instead of pristine graphene, which requires the use of toxic hydrazine vapor, and high-temperature annealing above 400 °C under an inert gas atmosphere to transform graphene oxide (GO) into RGO.[40] RGO is much easier to disperse in solvents and can give monolayer RGO in large quantities in comparison to GO, since RGOs chemically functionalized groups of oxides provide better solvent solubility and dispersion. However, large populations of defects still remain after the reduction, which seriously degrade the electronic properties.[41,42] Much higher quality graphene can be produced by liquid-phase exfoliation (LPE) of graphite powders using organic solvents as developed by Hernandez et al.[43] and O'Neill et al.[44] When compared to the other high quality graphene production methods such as chemical vapor deposition (CVD), molecular beam epitaxy (MBE), and growth on SiC,[45] LPE with organic solvents is quick and low-cost making it an industrially scalable method. Thus via this technique, we can envisage having enhanced graphene nanocomposites applied to a range of applications.

Here we develop a low-temperature processed nanocomposites of pristine graphene nanoflakes and anatase-TiO_2 nanoparticles and employ it as the electron selective contact in perovskite MSSCs. We observe reduced series resistance and unexpectedly reduced recombination losses with the low temperature composite. The resulting sub-150 °C processed MSSCs exhibit up to 15.6% power conversion efficiency. Slightly higher than the previously high-temperature sintered devices due to the superior properties of the graphene-TiO_2 nanocomposites.

To gain a better insight into the intrinsic properties of the starting materials, we performed detailed characterizations of graphene, TiO_2, and their nanocomposites. We produced graphene from graphite flakes by LPE with isopropanol as the dispersant, under sonication for up to 70 h. The detailed synthetic procedure has been described elsewhere.[44] We performed Raman spectroscopy and atomic force microscopy (AFM) to probe the graphene film quality and the number of graphene layers in each flake. The samples were prepared on SiO_2 substrates by drop casting the graphene solution and heating on a hot plate at 100 °C. Figure 1a shows the Raman spectrum for samples with decreasing flake size, controlled by increasing sonication time. Raman spectra give unique peaks for graphite materials. The two most prominent peaks are the G band (~1580 cm^{-1}) and the 2D band (~2700 cm^{-1}) as expected. We observe a difference in the contribution to the 2D band's shape from multiple peaks between exfoliated graphene flakes and starting graphite, suggesting our prepared samples are few-layer graphene.[46] In addition, we observed increased intensity for the peaks of the D band (~1350 cm^{-1}), progressing from the graphite flakes toward graphene. The reason for the appearance of the D band is that exfoliating graphite into graphene produces progressively smaller flakes with increasing sonication. We see that the intensity ratio of the D and G peaks (I_D/I_G) increases from graphite (I_D/I_G = 0.14) as it is converted into graphene flakes (I_D/I_G = 0.3), then increases further (I_D/I_G = 0.52) during continuous sonication. O'Neill et al., following the same technique, found that this was caused by a variation in flake size.[44] They suggest that liquid phase exfoliation of graphene causes the flake size to decrease and therefore the area/perimeter ratio to decrease, increasing the contribution of flake edges to the Raman spectrum. Because the D band not only represents the defects of graphene, but also the edges, more exposed edges increases the I_D/I_G ratio.[46]

The AFM image of exfoliated graphene flakes in Figure 1b allows us to have an approximate overview of the graphene morphology and its number of layers. It can be seen that the graphene flakes are distributed randomly over the substrate. The dimension of flakes varies between 0.1 and 1 μm. We also performed cross-sectional analysis of the graphene flakes, where we show a representative flake with a height of ~3.1 nm in the inset to Figure 1. We thus estimate that we have sheets of approximately five layers of graphene.[47] As reported in the

dx.doi.org/10.1021/nl403997a | Nano Lett. XXXX, XXX, XXX−XXX

literature, solution deposition of a graphene film onto SiO_2 can cause aggregation of the flakes. Therefore, although we observe very few monolayer flakes in our sample on SiO_2, this may give an overestimate of number of layers in the graphene flakes in our final nanocomposites films. Our Raman and AFM characterization are in good agreement with previous work, indicating high quality graphene synthesis without introducing significant defects via oxidation, and as prepared graphene is comparable to defect-free graphene.[43,44]

We prepared anatase TiO_2 nanoparticles following a hydrothermal method with the characterization and a detailed description given in the Supporting Information. The TiO_2 nanoparticles were approximately 25 nm in diameter and were blended with the graphene dispersion. From the SEM image in Figure 1c, we show the exposed surface of the nanocomposite highlighting TiO_2 nanoparticles anchored upon a graphene nanoflake. With graphene's remarkable conductivity it may serve as a highway for electron transportation and collection. We show in Supporting Information Figure S2a–d a detailed comparison between SEM micrographs of layers consisting of TiO_2 nanoparticles only and graphene-TiO_2 nanocomposites prepared on glass microscope slides.

Apart from the high-temperature processing limitation, another key issue in performance of the MSSC at present is the minimization of the series resistance. The compact n-type TiO_2 charge collection layers may significantly contribute to series resistance, as has been previously observed in solid-state DSSCs and planar heterojunction perovskite solar cells.[48,49] Following characterization of the nanocomposite materials, we investigate the performance of graphene-TiO_2 nanocomposites as n-type charge collection electrodes. We fabricated a series of solar cells with a varying content of graphene flakes in the composite to assess its impact. We show the full device architecture in a color-enhanced cross-sectional scanning electron microscopy (SEM) image and a schematic illustration of the device architecture along with an energy level diagram in Figure 2. All the devices here were fabricated on cleaned fluorine doped tin oxide (FTO) coated glass serving as the transparent electrode and substrate. We deposit the n-type collection layer of ~100 nm thickness by spin-coating from an isopropanol solution of a blend of graphene and TiO_2. We note that upon careful sonication before spin-coating, we produce a dense and well-distributed nanocomposite, with graphene acting as a continuous 2D conductive framework, allowing TiO_2 nanoparticles to anchor onto the graphene nanoflakes (See Supporting Information Figure S4 for TiO_2 nanoparticles coverage on graphene). Following deposition of a ~400 nm Al_2O_3 nanoparticle mesostructure from an isopropanol solution, $CH_3NH_3PbI_{3-x}Cl_x$ perovskite was deposited by spin-coating its precursor solution in DMF onto a warmed substrate, resulting in an infiltration of the perovskite within the mesostructure with the addition of a capping layer (around 350 nm). The main difference between the devices studied here and those reported by Ball et al.[10] is the additional capping layers of perovskite which results from coating upon a warm substrate. Then we deposited 2,2′,7,7′-tetrakis-(N,N-di-p-methoxyphenylamine)9,9′-spirobifluorene (Spiro-OMeTAD) as the hole-transporter material (HTM). Finally, devices were completed by thermal evaporation of gold contacts.

In order to optimize the devices, we varied the content of graphene in the TiO_2-graphene composite. The mean solar cell performance parameters for a batch of 83 devices, extracted from current–voltage curves measured under simulated AM 1.5, 106.5 mW/cm^2 sunlight are shown in Figure 3. We can see a clear trend of device enhancement by the introduction of graphene. Starting from the neat TiO_2 nanoparticles (NPs only), the average short-circuit current density (J_{sc}) and fill factor (FF) are around 13 mA/cm^2 and 0.56, respectively. With increasing graphene concentration in the electron collection layer, both the J_{sc} and FF increase up to average values of around 18.5 mA/cm^2 and 0.7, respectively, peaking at 0.6 wt %, followed by a decrease with further increases of graphene content. However, in contrast to the J_{sc} and FF, the average open circuit voltage (V_{oc}) only increased slightly with graphene's addition to the TiO_2 with an average V_{oc} of around 1 V up to 0.8 wt %. V_{oc} begins to decrease as the graphene concentration increases over 0.8 wt %, probably due to bare graphene contacting the perovskite directly, resulting in a less selective electrode, that is, recombination directly between the electrons in the graphene and holes in the perovskite. This is consistent with our estimate in the Supporting Information that the optimum graphene content of 0.6 wt % corresponds to just over 1 monolayer coverage of the graphene by TiO_2 nanoparticles. Hence, the power conversion efficiency (PCE), $\eta = J_{sc} \cdot V_{oc} \cdot FF / P_{in}$, where P_{in} is incident solar irradiance peaks with an average PCE value around 12.4%.

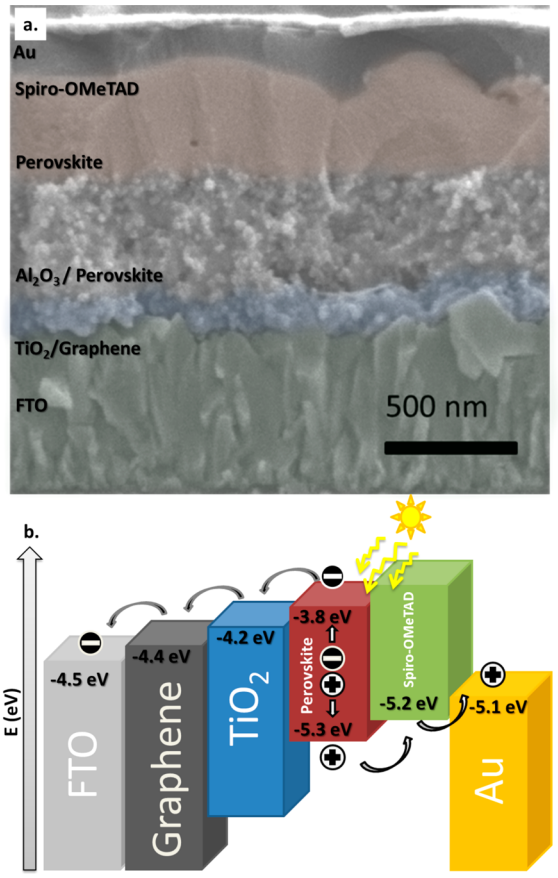

Figure 2. (a) Cross-sectional SEM micrographs with color-enhanced and annotated cross-section showing a general schematic of the solar cell architecture. (b) Schematic illustration of energy levels of the materials used in this study. We note that these are the energy levels of the individual materials, and upon contact within the solar cell there is likely to be a considerable relative shift.[50] We also note that the graphene and TiO_2 are blended into a single composite layer and not layered as depicted in the energy level diagram.

dx.doi.org/10.1021/nl403997a | Nano Lett. XXXX, XXX, XXX–XXX

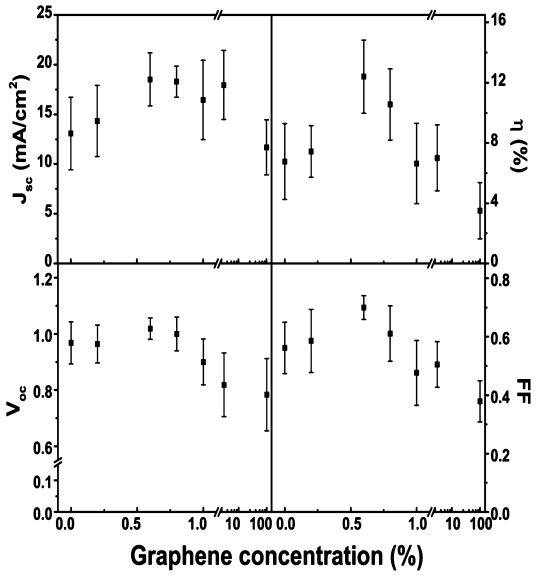

Figure 3. Graphene-concentration dependence in the nanocomposites of the parameters extracted from a single batch current–voltage measurements of solar cells under simulated AM 1.5, 106.5 mW/cm^2 irradiance.

In Figure 4a, we show the current density–voltage (J–V) curves of the best performing cells of each series, including cells with only neat TiO_2, neat graphene, high-temperature sintered TiO_2, and no n-type charge collection layer at all (just FTO). As can be seen in the J–V curves and the summarized performance parameters in Table 1, devices without any electron collection layer in the device architecture have inferior performance, but they do work. One of the main losses for the perovskite device coated directly upon the FTO conducting glass is fill factor, presumably due to an unfavorable electronic contact forming at the FTO perovskite interface. The electron collection layers with either neat graphene or low-temperature-processed TiO_2 nanoparticles show an improvement to J_{sc} and FF over the devices fabricated directly on FTO. We see further enhancement when we combine the graphene and TiO_2 nanoparticles together as a nanocomposites. The most efficient low-temperature processed perovskite MSSC based on a graphene-TiO_2 nanocomposite electron collection layer, exhibits a short-circuit photocurrent of 21.9 mA/cm^2, open-circuit voltage of 1.05 V, and a very high fill factor of 0.73 yielding a power conversion efficiency of 15.6%, (under 106.5 mW cm^{-2}) which is the best reported low-temperature solution-processed solar cell matching the highest reported efficiency of perovskite-based solar cells fabricated at either high temperature or by vapor deposition.[11,51] In addition, to the best of our knowledge the best performing solar cells incorporating graphene as a contact to crystalline Si remain at a power conversion efficiency of 14.5%,[52] hence our work here also sets a new milestone for the photovoltaic applications of graphene. In Supporting Information Figure S5, we show histograms of the solar cell performance parameters for the best devices, highlighting their reproducibility.

To disentangle any ambiguity in the variation of light absorption and its contribution to J_{sc} with varying graphene content we measured the light harvesting efficiency (LHE) of the solar cell active layers. Supporting Information Figure S7a shows the LHE for different graphene concentrations indicating only minor variation between films that cannot account for the observed J_{sc} variation. An example spectrum showing light extinction in each solar cell layer is presented in Supporting Information Figure S7b, along with estimates of the wavelength-averaged internal quantum efficiency (IQE) in Supporting Information Figure S7c. We conclude therefore that the changes in the photocurrent density between the samples are not due to changes in the total light absorbed in the perovskite layers.

Enhancements in the efficiency can be attributed to the improved V_{oc}, J_{sc}, and FF and may stem from beneficial factors resulting from synergetic effects between graphene and TiO_2 nanoparticles. As graphene has a work function between that of FTO and the TiO_2 conduction band, it may reduce the formation of energy barriers at the material interfaces and therefore behave as a better electron collector than with TiO_2 alone.[53] Second, the superior charge mobility of graphene may provide improved electrical conductivity of the layer. From the

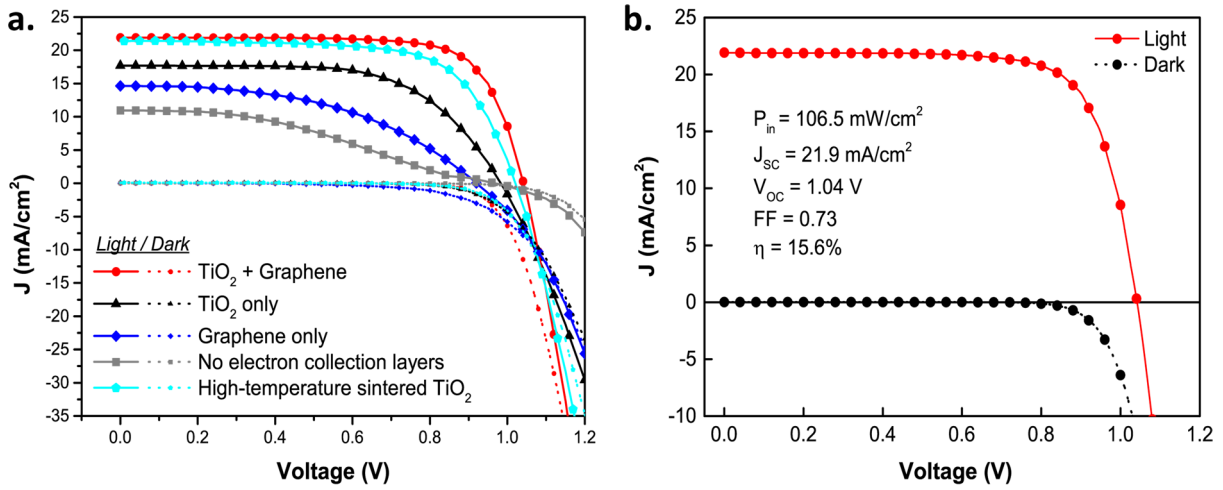

Figure 4. (a) Current–voltage characteristics of different electron collection layers under simulated AM 1.5, 100 mW/cm^2 solar irradiation (solid line), and in the dark (dotted line). (b) The best performing (η = 15.6%) solar cell based on a graphene-TiO_2 nanocomposites under simulated AM 1.5, 106.5 mW/cm^2 solar irradiation (solid line), and in the dark (dotted line), which processed at temperatures not exceeding 150 °C. Solar cell performance parameters are given in the inset.

dx.doi.org/10.1021/nl403997a | Nano Lett. XXXX, XXX, XXX–XXX

Table 1. Best Performance of Photovoltaics Based on Different Electron Collection Layer in This Study under Simulated AM 1.5, 106.5 mW/cm^2 Solar Irradiation

sample	J_{sc} (mA/cm^2)	V_{oc} (V)	FF	PCE (%)	R_s (Ohm·cm^2)
TiO_2 + graphene	21.9	1.04	0.73	15.6	4.3
TiO_2 only	17.7	1.00	0.61	10.0	10.1
graphene only	14.6	0.90	0.48	5.9	20.3
no electron collection layer	10.8	0.95	0.37	3.7	79.1
high-temperature sintered TiO_2	21.4	1.00	0.70	14.1	5.9

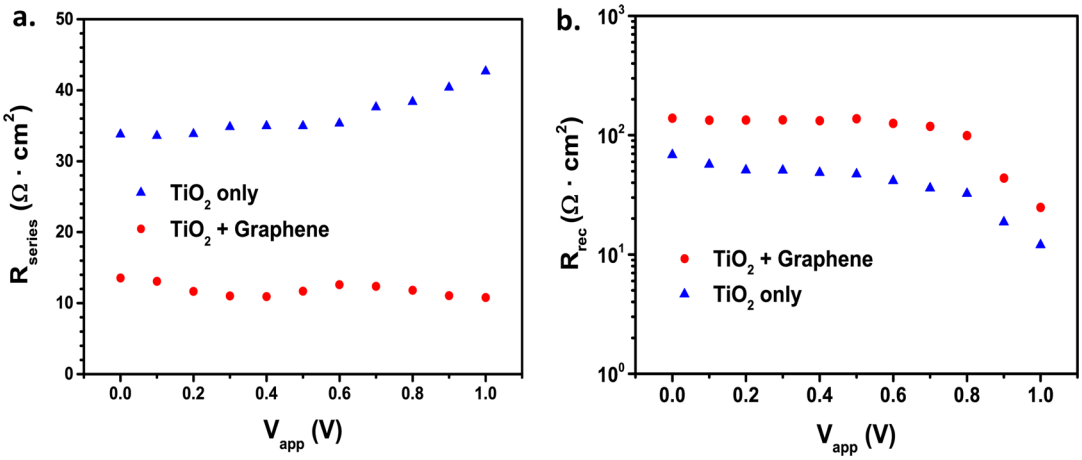

Figure 5. (a) Series resistance, R_{series}, and (b) recombination resistance, R_{rec}, obtained from impedance spectroscopy analysis of samples with two different concentrations of graphene mixed with TiO_2 in the electron collection layer.

very high fill factor, it is clear that the graphene/TiO_2 composite reduces the series resistance as compared to neat TiO_2 or even the conventional sintered TiO_2 collection layers. We can quantify the series resistance in the solar cell from the reciprocal value of the linear slope of the $J-V$ curves near the open-circuit voltage. We observe a decrease in the series resistance (R_{series}) to only 4 Ωcm^{-2}, as listed in the Table 1. This reduced series resistance has a striking impact upon the device FF.[54]

In order to further investigate the role of graphene addition to the observed enhanced solar cell performance, we performed impedance spectroscopy (IS) characterization on solar cells under working cell conditions (1 sun illumination). In previous work, the methodology and analysis of the Impedance spectroscopy is described in detail.[55] From these measurements we can extract the series resistance in the device, R_{series}, and the recombination resistance, R_{rec}. The R_{rec} explicitly relates to the component of resistance under forward bias due to electron and hole recombination within the solar cell. Our results are shown in Figure 5, where we observed that the addition of graphene reduces the series resistance in the cell, consistent with that extracted from the JV curves. This is consistent with an increase of the conductivity of the n-type collection layers or to a reduction in a contact resistance, either at the Perovskite/n-type layer, or n-type layers/FTO interface. The reduction in R_{series} in the devices is consistent with the JV curves and explains the increase in FF and efficiency.

A second factor leading to improved performance is the recombination resistance, R_{rec}, which we show to increase with the graphene-TiO2 composite in Figure 5b.[55,56] We would envisage that the highly conductive graphene should introduce new recombination centers and indeed the lower photocurrent in the graphene only devices is consistent with this. However, if the graphene flakes are fully coated with TiO_2 nanoparticles, then there should be no, or limited direct contact between the graphene and the perovskite. Previously, it has been observed that TiO_2 nanoparticles will undergo efficient electron transfer to graphene.[40] Hence, we postulate that in the graphene TiO_2 composite, most of the electron density will reside on the graphene and the ensuing "depleted" TiO_2 contacting the perovskite will have a lower recombination rate with the holes in the perovskite due to the reduced electron density in the TiO_2, thus contributing to the increase in the photocurrent under working conditions.

In conclusion, we have demonstrated the successful combination of two emerging materials, graphene and organometal trihalide perovskites, in solar cells. By exploiting nanocomposites of high quality graphene flakes and presynthesized TiO_2 nanoparticles in perovskite solar cells as a low-temperature processed electron collection layer, we have achieved a remarkable power conversion efficiency of 15.6%. This is the best recorded efficiency for low-temperature processed solar cells to date and matches the highest reported efficiency of high-temperature processed perovskite solar cells. This work also sets a milestone for incorporation of graphene in solar cells. This finding indicates that high-efficiency solar cells no longer need a high-temperature sintering process for TiO_2 as the electron collection layer. By combining with the fast printing deposition methods, the graphene/TiO_2 nanocomposite is ready to be compatible with reel-to-reel process and meet the needs of large scale industrial manufacture on a range of substrates and multilayer architectures.

■ ASSOCIATED CONTENT

Ⓢ Supporting Information

Full experimental methods, X-ray diffraction of TiO_2 nanoparticles, SEM micrographs of electron-selective layers, calculation of TiO_2 nanoparticle coverage on graphene, device

dx.doi.org/10.1021/nl403997a | Nano Lett. XXXX, XXX, XXX−XXX

reproducibility, device characteristics, and cumulative light extinction and internal quantum efficiency. This material is available free of charge via the Internet at http://pubs.acs.org.

AUTHOR INFORMATION

Corresponding Authors

*(R.J.N.) E-mail: r.nicholas1@physics.ox.ac.uk.
*(H.J.S.) E-mail: h.snaith1@physics.ox.ac.uk.

Author Contributions

The manuscript was written through contributions of all authors. All authors have given approval to the final version of the manuscript.

Notes

The authors declare no competing financial interest.

ACKNOWLEDGMENTS

This work was funded by EPSRC, UK. The authors thank Jin Zhang for experimental assistance. J.T.-W.W. would like to acknowledge Swire Educational Trust for supporting his DPhil study at Oxford. J.M.B. and H.J.S. acknowledge the European Union Seventh Framework Programme under the SANS project (grant 246124), and DESTINY project (grant 316494). A.A. thanks the EPSRC APEX project for financial support. E.M.B, I.M.-S., and J.B. acknowledge support by a project from Generalitat Valenciana (PROMETEO/2009/058).

REFERENCES

(1) Green, M. A.; Emery, K.; Hishikawa, Y.; Warta, W.; Dunlop, E. D. *Progr. Photovoltaics* **2013**, *21* (1), 1−11.
(2) Jackson, P.; Hariskos, D.; Lotter, E.; Paetel, S.; Wuerz, R.; Menner, R.; Wischmann, W.; Powalla, M. *Progr. Photovoltaics* **2011**, *19* (7), 894−897.
(3) Britt, J.; Ferekides, C. *Appl. Phys. Lett.* **1993**, *62* (22), 2851−2852.
(4) Nozik, A. J. *Physica E* **2002**, *14* (1−2), 115−120.
(5) Oregan, B.; Gratzel, M. *Nature* **1991**, *353* (6346), 737−740.
(6) Yu, G.; Gao, J.; Hummelen, J. C.; Wudl, F.; Heeger, A. J. *Science* **1995**, *270* (5243), 1789−1791.
(7) Lee, M. M.; Teuscher, J.; Miyasaka, T.; Murakami, T. N.; Snaith, H. J. *Science* **2012**, *338* (6107), 643−7.
(8) Kim, H. S.; Lee, C. R.; Im, J. H.; Lee, K. B.; Moehl, T.; Marchioro, A.; Moon, S. J.; Humphry-Baker, R.; Yum, J. H.; Moser, J. E.; Gratzel, M.; Park, N. G. *Sci. Rep.* **2012**, *2*, 591.
(9) Noh, J. H.; Im, S. H.; Heo, J. H.; Mandal, T. N.; Seok, S. I. *Nano Lett.* **2013**, *13* (4), 1764−9.
(10) Ball, J. M.; Lee, M. M.; Hey, A.; Snaith, H. J. *Energy Environ. Sci.* **2013**, *6* (6), 1739.
(11) Burschka, J.; Pellet, N.; Moon, S. J.; Humphry-Baker, R.; Gao, P.; Nazeeruddin, M. K.; Gratzel, M. *Nature* **2013**, *499* (7458), 316−9.
(12) Snaith, H. J. *J. Phys. Chem. Lett.* **2013**, *4* (21), 3623−3630.
(13) Graetzel, M.; Janssen, R. A. J.; Mitzi, D. B.; Sargent, E. H. *Nature* **2012**, *488* (7411), 304−312.
(14) Thavasi, V.; Renugopalakrishnan, V.; Jose, R.; Ramakrishna, S. *Mater. Sci. Eng. R* **2009**, *63* (3), 81−99.
(15) Ong, B. S.; Li, C. S.; Li, Y. N.; Wu, Y. L.; Loutfy, R. *J. Am. Chem. Soc.* **2007**, *129* (10), 2750−2751.
(16) Beiley, Z. M.; McGehee, M. D. *Energy Environ. Sci.* **2012**, *5* (11), 9173−9179.
(17) Muñoz-Rojas, D.; Sun, H.; Iza, D. C.; Weickert, J.; Chen, L.; Wang, H.; Schmidt-Mende, L.; MacManus-Driscoll, J. L. *Progr. Photovoltaics* **2013**, 393−400.
(18) Durr, M.; Schmid, A.; Obermaier, M.; Rosselli, S.; Yasuda, A.; Nelles, G. *Nat. Mater.* **2005**, *4* (8), 607−11.
(19) Hu, X.; Li, G.; Yu, J. C. *Langmuir* **2010**, *26* (5), 3031−3039.
(20) Weerasinghe, H. C.; Sirimanne, P. M.; Franks, G. V.; Simon, G. P.; Cheng, Y. B. *J. Photochem. Photobiol., A* **2010**, *213* (1), 30−36.
(21) Gong, J.; Liang, J.; Sumathy, K. *Renewable Sustainable Energy Rev.* **2012**, *16* (8), 5848−5860.
(22) Park, N. G.; van de Lagemaat, J.; Frank, A. J. *J. Phys. Chem. B* **2000**, *104* (38), 8989−8994.
(23) Weerasinghe, H. C.; Huang, F.; Cheng, Y.-B. *Nano Energy* **2013**, *2* (2), 174−189.
(24) Ito, S.; Ha, N.-L. C.; Rothenberger, G.; Liska, P.; Comte, P.; Zakeeruddin, S. M.; Pechy, P.; Nazeeruddin, M. K.; Graetzel, M. *Chem. Commun.* **2006**, *38*, 4004−4006.
(25) Chen, J.-H.; Jang, C.; Xiao, S.; Ishigami, M.; Fuhrer, M. S. *Nat. Nanotechnol.* **2008**, *3* (4), 206−209.
(26) Geim, A. K.; Novoselov, K. S. *Nat. Mater.* **2007**, *6* (3), 183−191.
(27) Morozov, S. V.; Novoselov, K. S.; Katsnelson, M. I.; Schedin, F.; Elias, D. C.; Jaszczak, J. A.; Geim, A. K. *Phys. Rev. Lett.* **2008**, *100* (1), 016602.
(28) Lee, C.; Wei, X.; Kysar, J. W.; Hone, J. *Science* **2008**, *321* (5887), 385−388.
(29) Chen, S.; Wu, Q.; Mishra, C.; Kang, J.; Zhang, H.; Cho, K.; Cai, W.; Balandin, A. A.; Ruoff, R. S. *Nat. Mater.* **2012**, *11* (3), 203−207.
(30) Balandin, A. A.; Ghosh, S.; Bao, W.; Calizo, I.; Teweldebrhan, D.; Miao, F.; Lau, C. N. *Nano Lett.* **2008**, *8* (3), 902−907.
(31) Nair, R. R.; Blake, P.; Grigorenko, A. N.; Novoselov, K. S.; Booth, T. J.; Stauber, T.; Peres, N. M. R.; Geim, A. K. *Science* **2008**, *320* (5881), 1308−1308.
(32) He, Q. Y.; Wu, S. X.; Yin, Z. Y.; Zhang, H. *Chem. Sci.* **2012**, *3* (6), 1764−1772.
(33) Huang, X.; Zeng, Z.; Fan, Z.; Liu, J.; Zhang, H. *Adv. Mater.* **2012**, *24* (45), 5979−6004.
(34) Huang, X.; Qi, X.; Boey, F.; Zhang, H. *Chem. Soc. Rev.* **2012**, *41* (2), 666−86.
(35) Yin, Z.; Zhu, J.; He, Q.; Cao, X.; Tan, C.; Chen, H.; Yan, Q.; Zhang, H. *Adv. Energy Mater.* **2013**, in press.
(36) Wu, S.; He, Q.; Tan, C.; Wang, Y.; Zhang, H. *Small* **2013**, *9* (8), 1160−72.
(37) Zhang, Y.; Tang, Z. R.; Fu, X.; Xu, Y. J. *ACS Nano* **2011**, *5* (9), 7426−35.
(38) Zhu, C.; Guo, S.; Wang, P.; Xing, L.; Fang, Y.; Zhai, Y.; Dong, S. *Chem. Commun. (Cambridge, U.K.))* **2010**, *46* (38), 7148−50.
(39) Liang, Y.; Wang, H.; Sanchez Casalongue, H.; Chen, Z.; Dai, H. *Nano Res.* **2010**, *3* (10), 701−705.
(40) Yang, N.; Zhai, J.; Wang, D.; Chen, Y.; Jiang, L. *ACS Nano* **2010**, *4* (2), 887−94.
(41) Pron, A.; Gawrys, P.; Zagorska, M.; Djurado, D.; Demadrille, R. *Chem. Soc. Rev.* **2010**, *39* (7), 2577−2632.
(42) Coleman, J. N. *Acc. Chem. Res.* **2013**, *46* (1), 14−22.
(43) Hernandez, Y.; Nicolosi, V.; Lotya, M.; Blighe, F. M.; Sun, Z.; De, S.; McGovern, I. T.; Holland, B.; Byrne, M.; Gun'Ko, Y. K.; Boland, J. J.; Niraj, P.; Duesberg, G.; Krishnamurthy, S.; Goodhue, R.; Hutchison, J.; Scardaci, V.; Ferrari, A. C.; Coleman, J. N. *Nat. Nanotechnol.* **2008**, *3* (9), 563−8.
(44) O'Neill, A.; Khan, U.; Nirmalraj, P. N.; Boland, J.; Coleman, J. N. *J. Phys. Chem. C* **2011**, *115* (13), 5422−5428.
(45) Bonaccorso, F.; Lombardo, A.; Hasan, T.; Sun, Z.; Colombo, L.; Ferrari, A. C. *Mater. Today* **2012**, *15* (12), 564−589.
(46) Ferrari, A. C.; Meyer, J. C.; Scardaci, V.; Casiraghi, C.; Lazzeri, M.; Mauri, F.; Piscanec, S.; Jiang, D.; Novoselov, K. S.; Roth, S.; Geim, A. K. *Phys. Rev. Lett.* **2006**, *97* (18), 187401.
(47) Novoselov, K. S.; Geim, A. K.; Morozov, S. V.; Jiang, D.; Zhang, Y.; Dubonos, S. V.; Grigorieva, I. V.; Firsov, A. A. *Science* **2004**, *306* (5696), 666−669.
(48) Eperon, G. E.; Burlakov, V. M.; Docampo, P.; Goriely, A.; Snaith, H. J. *Adv. Funct. Mater.* **2013**, in press.
(49) Liu, M.; Johnston, M. B.; Snaith, H. J. *Nature* **2013**, *501*, 395−398.
(50) Wang, X.; Zhi, L.; Muellen, K. *Nano Lett.* **2008**, *8* (1), 323−327.

(51) Novoselov, K. S.; Geim, A. K.; Morozov, S. V.; Jiang, D.; Katsnelson, M. I.; Grigorieva, I. V.; Dubonos, S. V.; Firsov, A. A. *Nature* **2005**, *438* (7065), 197−200.
(52) Shi, E. Z.; Li, H. B.; Yang, L.; Zhang, L. H.; Li, Z.; Li, P. X.; Shang, Y. Y.; Wu, S. T.; Li, X. M.; Wei, J. Q.; Wang, K. L.; Zhu, H. W.; Wu, D. H.; Fang, Y.; Cao, A. Y. *Nano Lett.* **2013**, *13* (4), 1776−1781.
(53) Snaith, H. J.; Gratzel, M. *Adv. Mater.* **2006**, *18* (14), 1910−1914.
(54) Nelson, J. *The Physics of Solar Cells*; Imperial College Press: London, 2003.
(55) Kim, H. S.; Mora-Sero, I.; Gonzalez-Pedro, V.; Fabregat-Santiago, F.; Juarez-Perez, E. J.; Park, N. G.; Bisquert, J. *Nat. Commun.* **2013**, *4*, 2242.
(56) Kim, H. S.; Lee, J. W.; Yantara, N.; Boix, P. P.; Kulkarni, S. A.; Mhaisalkar, S.; Gratzel, M.; Park, N. G. *Nano Lett.* **2013**, *13* (6), 2412−7.

dx.doi.org/10.1021/nl403997a | *Nano Lett.* XXXX, XXX, XXX−XXX